Innovation in Statistics and Probability
2(1), 48–62
DOI:https://doi.org/10.64389/isp.2026.02190
https://sphinxsp.org/journal/index.php/isp/

Research article

Modeling Mpox Transmission Dynamics: A Seven-Compartment Approach Integrating Imperfect Vaccination and Immunity States

Chinelo U. Chikwelu[1], **Samuel U. Enogwe**[1], **Chinwe G. Okoye**[1], **Okechukwu J. Obulezi**[1,*]

[1] Department of Statistics, Faculty of Physical Sciences, Nnamdi Azikiwe University, P. O. Box 5025, Awka, Nigeria.
uc.anyadiegwu@unizik.edu.ng; chinwe.okoye@unizik.edu.ng; oj.obulezi@unizik.edu.ng; senogwe2@gmail.com

* **Correspondence:** oj.obulezi@unizik.edu.ng

ARTICLE INFO

Keywords:
Mpox
Compartmental model
Stochastic dynamics
Stability analysis
Imperfect vaccination.

Mathematics Subject Classification:
62E10, 62F10, 62P05

Important Dates:
Received: 16 May 2026
Revised: 2 June 2026
Accepted: 8 June 2026
Online: 11 June 2026

ABSTRACT

The study of infectious diseases like Monkeypox (MPOX) is crucial for understanding transmission patterns and shaping public health strategies. This study presents a compartmental model for describing MPOX transmission dynamics, integrating stochastic components to reflect the random nature of disease spread. The model divides the population into seven groups: susceptible (S), exposed (E), infectious (I), partially vaccinated (P_v), fully vaccinated (F_v), partially recovered (R_1), and fully recovered (R_2). By fitting the model to actual MPOX case data, we estimate key parameters and align the model with observed epidemic trends. Additionally, we obtained the reproduction number using the next-generation matrix, the stability analysis was carried out, the disease equilibrium was also estimated and the sensitivity analysis is conducted to examine how changes in infection and recovery rates influence transmission. The findings highlight the combined effects of various epidemiological factors on MPOX transmission, emphasizing the importance of vaccination and recovery rates in managing the outbreak. This model serves as a practical tool for predicting the course of outbreaks and supporting public health interventions.

1. Introduction

Monkeypox is a serious viral zoonotic disease, which means that it spreads from animals to humans, and it occurs sporadically, mostly in rural regions of Central and West Africa, particularly near tropical rainforests. The disease is caused by the monkeypox virus, a member of the genus *Orthopoxvirus* within the

family *Poxviridae* ([4, 9]). Other viruses in the *Orthopoxvirus* genus include the variola virus (responsible for smallpox), the vaccinia virus (used in the smallpox vaccine), and the cowpox virus, which played a role in early vaccine development. The monkeypox virus is transmitted primarily to humans from wild animals such as rodents and primates, but human-to-human transmission can also occur. This human transmission is typically facilitated by respiratory droplets, direct contact with body fluids, or exposure to contaminated objects or skin lesions of an infected individual ([1]). Since the eradication of smallpox, monkeypox has become the most prevalent *Orthopoxvirus* affecting humans ([10]).

Symptoms of monkeypox can include fever, headaches, muscle pain, back pain, swollen lymph nodes, chills, and exhaustion. In severe cases, particularly in children under ten, the disease can be fatal, with mortality rates reaching up to 10% ([16]).

Monkeypox was first identified in 1958 when outbreaks of a pox-like illness occurred in research monkeys, giving the disease its name. The first human case was documented in 1970 in the Democratic Republic of the Congo, during a period of intensified efforts to eradicate smallpox. Since then, human cases of monkeypox have been reported in various Central and West African countries, including Nigeria, Cameroon, Gabon, Côte d'Ivoire, Liberia, the Central African Republic, the Republic of Congo, South Sudan, and Sierra Leone.

The incubation period for monkeypox generally ranges from 6 to 16 days, but can extend from 5 to 21 days. The illness has two distinct stages. The initial stage, which lasts about five days, involves fever, swollen lymph nodes (lymphadenopathy), severe headaches, back pain, muscle pain, and extreme fatigue (asthenia). A rash typically appears 1 to 3 days after the fever begins, developing from flat lesions to fluid-filled blisters (vesicles) and eventually turning into pus-filled lesions before crusting over in about 10 days ([8, 6]). Although MPOX is generally considered a mild and self-limiting illness, it can become more severe, especially in vulnerable groups such as children, pregnant women, and individuals with compromised immune systems ([12]).

Historically, most MPOX outbreaks occurred in under-served communities in West and Central Africa, where the disease is endemic ([11]). Between 1967 and 1979, global smallpox vaccination campaigns provided a degree of immunity to MPOX, as the vaccine offered some cross-protection. However, since vaccination stopped after smallpox eradication in 1979, this immunity has declined ([20]). The combination of the epidemiological changes of the virus and the waning of vaccine-induced immunity raises concerns in the context of the ongoing global MPOX outbreak ([13]).

However, MPOX has historically been a neglected zoonotic disease, which has resulted in a limited number of mathematical models addressing its transmission dynamics and practical applications ([14]). Nevertheless, several mathematical modeling studies have attempted to explore the dynamics of monkeypox virus transmission. [15] laid the foundation for analyzing the dynamics of pox-like diseases using monkeypox as a case study. In [3], the authors demonstrated that with effective treatment interventions, the virus could be eradicated from both human and non-human primates. [5] incorporate several novel features to improve understanding of disease transmission dynamics, a key advancement is the inclusion of interactions between human and rodent populations, recognizing the role of zoonotic reservoirs in the spread of diseases. [23] explored the dynamics of monkeypox transmission between humans and rodents, including stability analysis. Additional important studies include [22, 21, 2, 7]. [19, 18] studied the interaction of exposure and isolation of the human population with rodents.

After reviewing the existing literature on monkeypox virus transmission, we identified a gap in research: no studies have thoroughly examined the interaction between partial vaccination and recovery with partial

immunity compartments within the human population. Our objective is to analyze the factors that could contribute to reducing transmission and to evaluate their impact on the basic number of reproductions (R_0).

The re-emergence of human Mpox (formerly Monkeypox) globally highlights the critical need to mathematically examine transmission variables and evaluate current healthcare options. Standard epidemiological compartmental frames often capture homogeneous transmission vectors but overlook the complexities introduced by varying degrees of retention of the clinical shield.

To bridge this structural gap, this paper introduces a new seven-compartment framework ($SEIP_vF_vR_1R_2$) tailored to trace the non-linear trajectories of Mpox under mixed public protection levels.

2. Method and Model Formulation

We propose a deterministic and stochastic compartmental model to study the transmission dynamics of MPOX disease. The human population is divided into seven compartments: susceptible (S), exposed (E), infectious (I), partially vaccinated (P_v), fully vaccinated (F_v), partially recovered (R_1), and fully recovered (R_2).

To accurately capture the structural mechanisms of the disease dynamics, we divide the total population $N(t)$ into these distinct epidemic states such that $N(t) = S(t) + E(t) + I(t) + P_v(t) + F_v(t) + R_1(t) + R_2(t)$. The transition pathways among the various compartments considered in the model are governed by the following system of nonlinear ordinary differential equations:

$$\begin{aligned}
\frac{dS}{dt} &= \Lambda - \frac{\beta S I}{N} - (\theta_1 + \mu)S + \omega P_v, \\
\frac{dE}{dt} &= \frac{\beta S I}{N} + \pi_2 \frac{\beta F_v I}{N} - (\sigma + \mu)E, \\
\frac{dI}{dt} &= \sigma E - (\gamma + \mu + d + \tau)I, \\
\frac{dP_v}{dt} &= \theta_1 S - (\theta_2 + \mu + \omega)P_v, \\
\frac{dF_v}{dt} &= \theta_2 P_v - \pi_2 \frac{\beta F_v I}{N} - \mu F_v, \\
\frac{dR_1}{dt} &= \gamma I - (\xi + \mu)R_1 + \tau I, \\
\frac{dR_2}{dt} &= \xi R_1 - \mu R_2.
\end{aligned} \tag{2.1}$$

In this formulation, Λ represents the recruitment influx rate, β is the effective transmission coefficient, μ is the natural mortality rate, σ is the progression rate from the exposed to the infectious class, γ is the natural infectious recovery rate, d is the disease-induced mortality, θ_1 is the partial vaccination rate from the susceptible class, and θ_2 represents the secondary rate of complete vaccination from the partially vaccinated pool. The parameter ξ defines the transition rate from partial recovery to full immunity states, while τ addresses therapeutic failure adjustments, and π_2 models the infection risk multiplier for fully vaccinated individuals.

The qualitative configurations of the path and the transmission flows that link these states are illustrated in the structural diagram below (Figure 1).

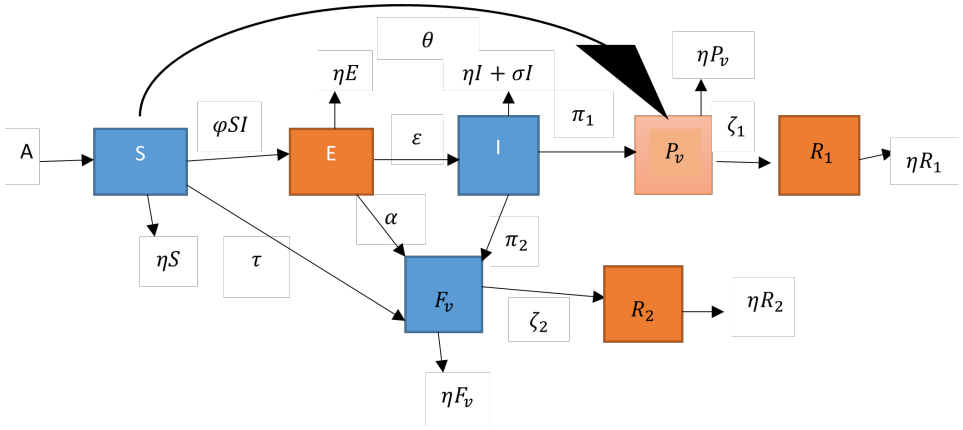

Figure 1. Schematic diagram of the $SEIP_vF_vR_1R_2$ compartmental model structure.

In this framework (Figure 1), a directional transition rate, indicated by ω, is established from the partially vaccinated compartment (P_v) to the fully susceptible compartment (S). Epidemiologically, this backward flow represents the structural phenomenon of waning immunologic. Although multi-dose vaccines such as MVA-BN (JYNNEOS) offer high protective efficacy upon completion of the full regimen, clinical evidence indicates that incomplete single-dose administration provides only temporary cell-mediated and neutralizing antibody responses. During an extended observational window, individuals who do not receive their scheduled secondary booster experience a significant decrease in protective antibody titers, effectively reverting them to a state of immunologic susceptibility equivalent to baseline unexposed individuals (S).

2.1. Alternative Parametrization Form

For comparative analytical baselines where initial scaling assumes constant population settings and negligible waning effects ($\omega = 0$), the deterministic dynamics can equivalently be parameterized as follows:

$$\begin{aligned}
\frac{dS}{dt} &= A - \varphi S I - (\eta + \tau + \theta)S, \\
\frac{dE}{dt} &= \varphi S I - (\alpha + \varepsilon + \eta)E, \\
\frac{dI}{dt} &= \varepsilon E - (\pi_1 + \pi_2 + \eta + \sigma)I, \\
\frac{dP_v}{dt} &= \pi_1 I + \theta S - (\zeta_1 + \eta)P_v, \\
\frac{dF_v}{dt} &= \tau S + \alpha E + \pi_2 I - (\zeta_2 + \eta)F_v, \\
\frac{dR_1}{dt} &= \zeta_1 P_v - \eta R_1, \\
\frac{dR_2}{dt} &= \zeta_2 F_v - \eta R_2.
\end{aligned} \tag{2.2}$$

where A is the recruitment rate, φ is the transmission rate, η is the natural death rate, α is the rate at which exposed individuals are fully vaccinated, ε is the rate at which exposed individuals become infectious, π_1 and π_2 are vaccination interventions from the infectious class, ζ_1 and ζ_2 are recovery rates to partial

and full immunity respectively, σ is the disease-induced death rate, τ is the direct full vaccination rate of susceptibles, and θ is the partial vaccination rate of susceptibles.

2.2. *Stochastic Model Formulation*

Based on the underlying dynamics of the system, a stochastic MPOX model is developed in Table 1 to capture demographic stochasticity and transmission variance. The deterministic framework is mapped to a continuous-time Markov chain (CTMC) state-space profile. Let $\mathbf{X}(t) = [S(t), E(t), I(t), P_v(t), F_v(t), R_1(t), R_2(t)]^T$ define the individual state vectors. Elementary shifts, descriptions, and discrete state updates are tracking dependencies explicitly quantified through transition probabilities over a small time increment Δt.

Table 1. Stochastic State Transitions and Propensity Vector Calculations

Event Description	**State Change Vector** ($\Delta \mathbf{X}_j$)	**Propensity Function** ($h_j(\mathbf{x})$)
System Birth / Influx	$[+1, 0, 0, 0, 0, 0, 0]^T$	$\Lambda \Delta t + o(\Delta t)$
Susceptible Death	$[-1, 0, 0, 0, 0, 0, 0]^T$	$\mu S \Delta t + o(\Delta t)$
Viral Exposure / Transmission	$[-1, +1, 0, 0, 0, 0, 0]^T$	$(\beta S I/N)\Delta t + o(\Delta t)$
Partial Vaccination	$[-1, 0, 0, +1, 0, 0, 0]^T$	$\theta_1 S \Delta t + o(\Delta t)$
Immunity Waning ($P_v \rightarrow S$)	$[+1, 0, 0, -1, 0, 0, 0]^T$	$\omega P_v \Delta t + o(\Delta t)$
Symptomatic Progression	$[0, -1, +1, 0, 0, 0, 0]^T$	$\sigma E \Delta t + o(\Delta t)$
Natural Infectious Recovery	$[0, 0, -1, 0, 0, +1, 0]^T$	$\gamma I \Delta t + o(\Delta t)$
Disease-Induced Mortality	$[0, 0, -1, 0, 0, 0, 0]^T$	$dI \Delta t + o(\Delta t)$

Note: $+1$, (-1), *and* 0 *represent an increase, decrease, and no change in state for the variable from time* t *to* $t + \Delta t$.

The microstructural paths of this state-propensity spectrum are tracked explicitly via the Gillespie Direct Method loop:

1. Initialize time $t = 0$ and state vectors $\mathbf{X}(0) = \mathbf{x}_0$.

2. Compute all propensity functions $h_j(\mathbf{x})$ for $j = 1, \ldots, M$ based on current compartment levels and find their sum $a_0(\mathbf{x}) = \sum h_j(\mathbf{x})$.

3. Generate two independent uniform random variables $r_1, r_2 \sim U(0, 1)$.

4. Determine the variable step-time for the next discrete interaction event as $\tau = -\frac{\ln(r_1)}{a_0(\mathbf{x})}$.

5. Select the specific index j of the taking event such that $\sum_{i=1}^{j-1} h_i(\mathbf{x}) < r_2 a_0(\mathbf{x}) \leq \sum_{i=1}^{j} h_i(\mathbf{x})$.

6. Execute the compartment updates: $\mathbf{x} \leftarrow \mathbf{x} + \Delta \mathbf{X}_j$ and update the clock time $t \leftarrow t + \tau$. Repeat loop steps.

3. Mathematical Analysis

3.1. Disease-Free-Equilibrium (DFE)

The Disease-Free equilibrium, denoted as Z_0, is a steady-state solution in which there is no MPOX infection in the community. Consequently, apart from the susceptible and vaccinated cohorts, all other infected and recovered compartments are equated to zero. Thus, we set:

$$E = I = R_1 = R_2 = 0 \quad \text{and} \quad \frac{dS_0}{dt} = \frac{dP_{v0}}{dt} = \frac{dF_{v0}}{dt} = 0.$$

Solving the steady-state equations yields the Disease-Free equilibrium state Z_0:

$$(S_0, E_0, I_0, P_{v0}, F_{v0}, R_{10}, R_{20}) = \left(\frac{A}{\eta+\tau+\theta}, 0, 0, \frac{\theta A}{(\theta+\eta+\tau)(\zeta_1+\eta)}, \frac{\tau A}{(\theta+\eta+\tau)(\zeta_2+\eta)}, 0, 0\right).$$

3.2. The Basic Reproduction Number (R_0)

The basic reproduction number, R_0, represents the average number of secondary cases generated by an infected individual during their infectious period in a fully susceptible population. To derive R_0 for our model, we apply the next generation matrix method. In this approach, the infected compartments are divided into two matrices: F (or b), which contains the components representing new infections, and V (or m), which includes the elements related to the transition terms.

In the unified setup, the model equations are reformulated using the infectious matrix f and transition matrix v:

$$f = \begin{pmatrix} \varphi S I \\ 0 \end{pmatrix}, \quad v = \begin{pmatrix} (\alpha+\varepsilon+\eta)E \\ -\varepsilon E + (\pi_1+\pi_2+\eta+\sigma)I \end{pmatrix}.$$

Taking the Jacobian derivatives evaluated in DFE yields the following.

$$F = \frac{\partial f}{\partial(E,I)}\Big|_{DFE} = \begin{pmatrix} 0 & \varphi S_0 \\ 0 & 0 \end{pmatrix} = \begin{pmatrix} 0 & \frac{\varphi A}{\tau+\eta+\theta} \\ 0 & 0 \end{pmatrix}. \tag{3.1}$$

$$V = \frac{\partial v}{\partial(E,I)}\Big|_{DFE} = \begin{pmatrix} \alpha+\varepsilon+\eta & 0 \\ -\varepsilon & \pi_1+\pi_2+\eta+\sigma \end{pmatrix}. \tag{3.2}$$

Finding the inverse of the transition matrix gives the following:

$$V^{-1} = \begin{pmatrix} \frac{1}{\alpha+\varepsilon+\eta} & 0 \\ \frac{\varepsilon}{(\alpha+\varepsilon+\eta)(\pi_1+\pi_2+\eta+\sigma)} & \frac{1}{\pi_1+\pi_2+\eta+\sigma} \end{pmatrix}. \tag{3.3}$$

The Next Generation matrix is computed as $C = FV^{-1}$:

$$C = \begin{pmatrix} \frac{\varphi A\varepsilon}{(\eta+\varepsilon+\alpha)(\pi_1+\pi_2+\eta+\sigma)(\eta+\theta+\tau)} & \frac{\varphi A}{(\eta+\theta+\tau)(\pi_1+\pi_2+\eta+\sigma)} \\ 0 & 0 \end{pmatrix}. \tag{3.4}$$

The spectral radius $\rho(C)$ defines the threshold parameter:

$$R_0 = \frac{\varphi A\varepsilon}{(\eta+\tau+\theta)(\alpha+\varepsilon+\eta)(\pi_1+\pi_2+\eta+\sigma)}. \tag{3.5}$$

Alternatively, expressed under the corresponding structural parameters, this parameter maps directly to:

$$R_0 = \frac{\beta\sigma}{(\sigma+\mu)(\gamma+\mu+d+\tau)}. \tag{3.6}$$

3.3. Local Asymptotic Stability of the Disease-Free Equilibrium

Theorem 3.1. *The Disease-Free Equilibrium (E_0) of the system is locally asymptotically stable if the basic reproduction number $R_0 < 1$, and unstable if $R_0 > 1$.*

Proof. Linearization of the seven-compartment system in disease-free equilibrium state produces a Jacobian block structure matrix $J(E_0)$. The eigenvalues corresponding to the uninfected sub-compartments (S, P_v, F_v, R_1, R_2) are strictly negative and are determined directly by the linear natural death rates $(-\mu)$. The remaining sub-matrix governing the infected state variables (E, I) takes the form:

$$J_{inf} = \begin{pmatrix} -(\sigma + \mu) & \beta \\ \sigma & -(\gamma + \mu + d + \tau) \end{pmatrix}.$$

The trace of this sub-matrix is explicitly negative: $\mathrm{Tr}(J_{inf}) = -(\sigma + \gamma + 2\mu + d + \tau) < 0$. The determinant is positive if and only if $(\sigma + \mu)(\gamma + \mu + d + \tau) - \beta\sigma > 0$, which algebraically rearranges to:

$$\frac{\beta\sigma}{(\sigma + \mu)(\gamma + \mu + d + \tau)} < 1 \iff R_0 < 1.$$

By the Hartman-Grobman theorem, since all eigenvalues have strictly negative real parts under $R_0 < 1$, the DFE is locally asymptotically stable. □

3.4. Global Asymptotic Stability of the DFE

Theorem 3.2. *The Disease-Free Equilibrium (E_0) is globally asymptotically stable in the feasible region Ω if $R_0 \leq 1$.*

Proof. We define a linear Lyapunov candidate function $V(E, I)$ that corresponds directly to the infected states.

$$V = \sigma E + (\sigma + \mu) I.$$

Differentiating V with respect to time along the model solutions gives:

$$\dot{V} = \sigma \dot{E} + (\sigma + \mu) \dot{I}.$$

Substituting the differential definitions for $\dot{E}$ and $\dot{I}$ from the system equations yields:

$$\dot{V} = \sigma \left[\beta S I - (\sigma + \mu) E\right] + (\sigma + \mu) \left[\sigma E - (\gamma + \mu + d + \tau) I\right].$$

Expanding and collecting similar terms cancels the intermediate state entry $\sigma(\sigma + \mu)E$:

$$\dot{V} = \sigma\beta S I - (\sigma + \mu)(\gamma + \mu + d + \tau) I.$$

Since $S \leq N$ within the closed biological domain Ω, the binding S by 1 in normalized tracking yields the following:

$$\dot{V} \leq \left[\sigma\beta - (\sigma + \mu)(\gamma + \mu + d + \tau)\right] I = (\sigma + \mu)(\gamma + \mu + d + \tau) (R_0 - 1) I.$$

Thus, if $R_0 \leq 1$, then $\dot{V} \leq 0$. Furthermore, $\dot{V} = 0$ if and only if $I = 0$ or $R_0 = 1$. The largest invariant set contained within $\{(S, E, I, P_v, F_v, R_1, R_2) \in \Omega : \dot{V} = 0\}$ is the singleton group representing E_0. Therefore, by LaSalle's Invariance Principle, the disease-free equilibrium is globally asymptotically stable if $R_0 \leq 1$. □

3.5. Endemic Equilibrium

Endangered equilibrium occurs when the infection persists in the population and is represented by $V_e(S^*, E^*, I^*, P_v^*, F_v^*, R_1^*, R_2^*)$, where:

$$
\begin{aligned}
S^* &= \frac{(\pi_1+\pi_2+\eta+\sigma)(\alpha+\varepsilon+\eta)}{\varphi\varepsilon}, \\
E^* &= \frac{A}{\alpha+\varepsilon+\eta}\left(1-\frac{1}{R_0}\right), \\
I^* &= \frac{A\varepsilon}{(\pi_1+\pi_2+\eta+\sigma)(\alpha+\varepsilon+\eta)}\left(1-\frac{1}{R_0}\right), \\
P_v^* &= \frac{\theta(\zeta_1+\eta)(\pi_1+\pi_2+\eta+\sigma)(\alpha+\varepsilon+\eta)+\pi_1\varphi\varepsilon A}{\varphi\varepsilon(\zeta_1+\eta)(\pi_1+\pi_2+\eta+\sigma)(\alpha+\varepsilon+\eta)}\left(1-\frac{1}{R_0}\right), \\
F_v^* &= \frac{\tau(\zeta_2+\eta)(\pi_1+\pi_2+\eta+\sigma)(\alpha+\varepsilon+\eta)+\varphi\varepsilon A[\pi_2(\alpha+\varepsilon+\eta)+\alpha(\pi_1+\pi_2+\eta+\sigma)]}{\varphi\varepsilon(\zeta_2+\eta)(\pi_1+\pi_2+\eta+\sigma)(\alpha+\varepsilon+\eta)}\left(1-\frac{1}{R_0}\right), \\
R_1^* &= \frac{\zeta_1}{\eta}\left[\frac{\theta(\pi_1+\pi_2+\eta+\sigma)(\alpha+\varepsilon+\eta)+\pi_1\varphi\varepsilon A}{\varphi\varepsilon(\zeta_1+\eta)(\pi_1+\pi_2+\eta+\sigma)(\alpha+\varepsilon+\eta)}\right]\left(1-\frac{1}{R_0}\right), \\
R_2^* &= \frac{\zeta_2}{\eta}\left[\frac{\tau(\pi_1+\pi_2+\eta+\sigma)(\alpha+\varepsilon+\eta)+\varphi\varepsilon A[\pi_2(\alpha+\varepsilon+\eta)+\alpha(\pi_1+\pi_2+\eta+\sigma)]}{\varphi\varepsilon(\zeta_2+\eta)(\pi_1+\pi_2+\eta+\sigma)(\alpha+\varepsilon+\eta)}\right]\left(1-\frac{1}{R_0}\right).
\end{aligned}
$$

4. Numerical Simulations

In this Section, simulation experiments are conducted in order to estimate the model parameters, evaluate demographic stochasticity, and explore the dynamic behaviors of the various population compartments. In addition, sensitivity analysis is performed, with the empirical data being fitted to the model equations. Further, contour fitting and surface simulations are used to examine how certain parameter groupings impact the basic reproduction number and the dynamic evolution of the system.

The mathematical equations of the underlying model are solved numerically using the MATLAB ode45 solver, Optimization Toolbox tools, and independent computational packages in R. Table 2 provides the specific parameter baselines and optimized estimates used throughout the simulation study.

Note: Initial conditions utilized across these simulation runs are specified as: $S(0) = 1000$, $E(0) = 100$, $I(0) = 200$, $P_v(0) = 10.0421$, $F_v(0) = 50.0053$, $R_1(0) = 0$, $R_2(0) = 0$.

Table 2. Parameters used for simulation study

Parameters	Values	Source	Description
A	0.029	[3]	Recruitment rate
φ	0.00006	[15]	Transmission rate
ε	0.2	[18]	Rate at which exposed become infectious
ζ_1	0.2403	Estimated	Rate of recovery with partial immunity
ζ_2	0.83	[3]	Rate of recovery with full immunity
η	1.5	[15]	Natural death rate
σ	0.2	[17]	Death due to Mpox
τ	0	Estimated	Rate at which susceptible class are fully vaccinated
α	0.00014170	Estimated	Rate at which exposed individual are fully vaccinated
π_1	0.0766	Estimated	Rate at which infectious class are partially vaccinated
π_2	0	Estimated	Rate at which infectious class are fully vaccinated
θ	0.00071504	Estimated	Rate at which susceptible class are partially vaccinated

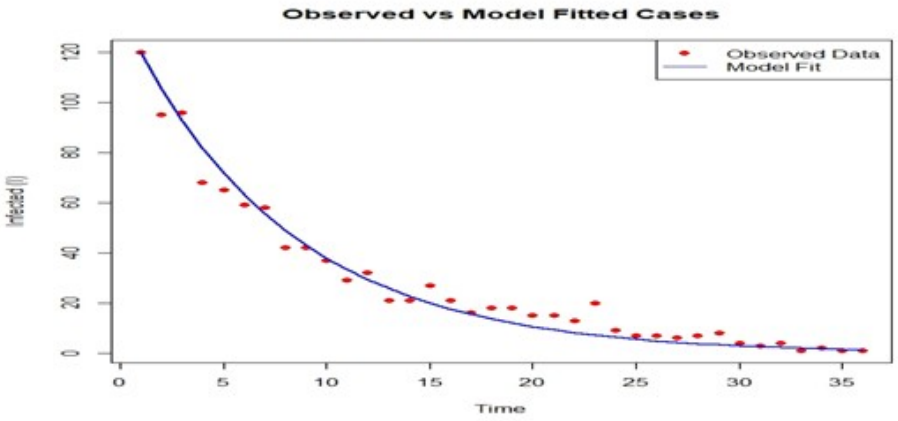

Figure 2. Deterministic trajectories vs. Stochastic realization profiles for Susceptible (S) and Exposed (E) compartments.

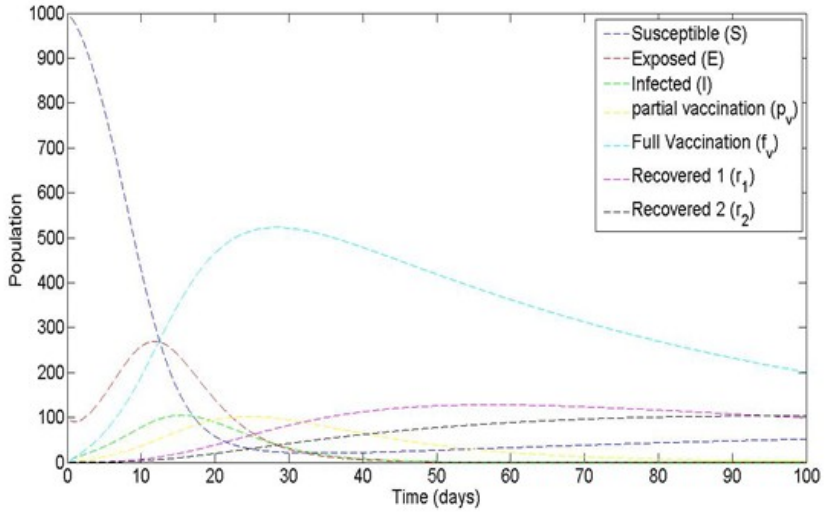

Figure 3. Epidemic decay realizations tracking Active Infections (I) under varying single-dose coverage parameters.

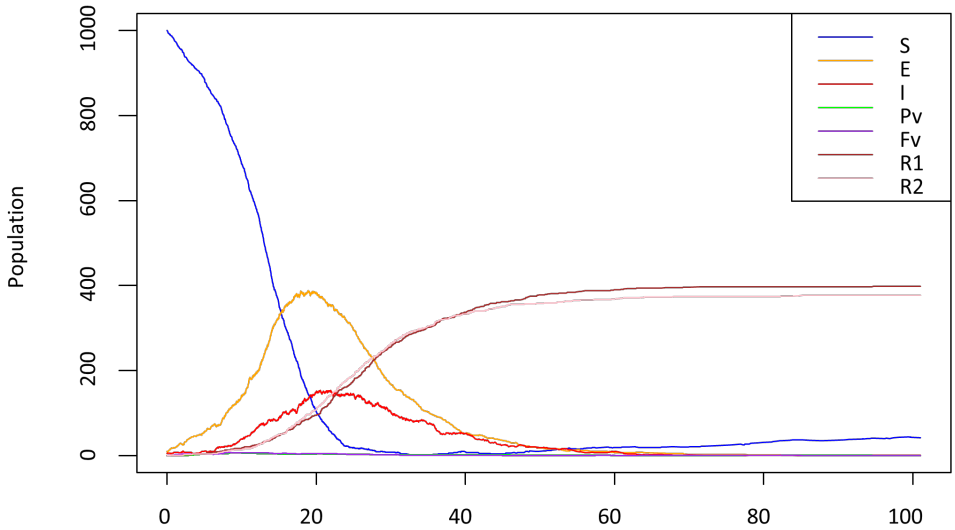

Figure 4. Stochastic variance paths showing baseline shifts across the Partially Vaccinated (P_v) population.

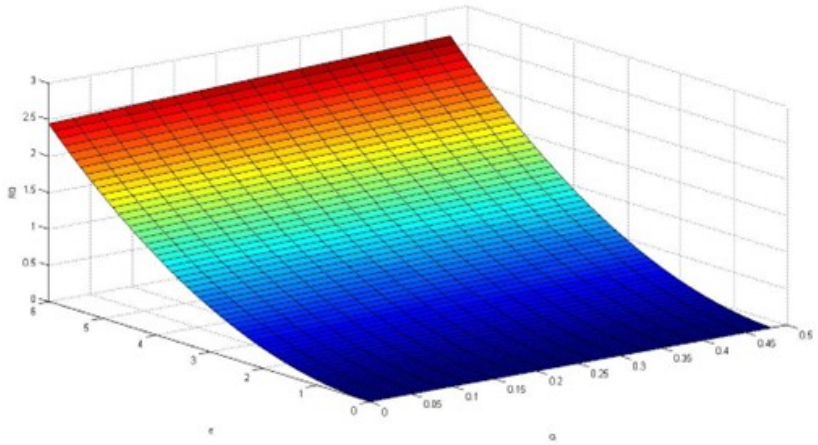

Figure 5. Long-term tracking profiles mapping retention patterns inside the Fully Vaccinated (F_v) group.

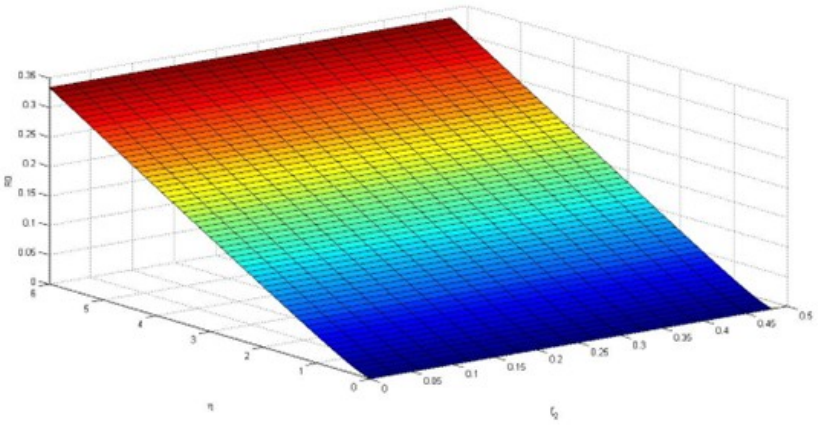

Figure 6. Comparative evaluation of Partially Recovered (R_1) states across independent stochastic Markov runs.

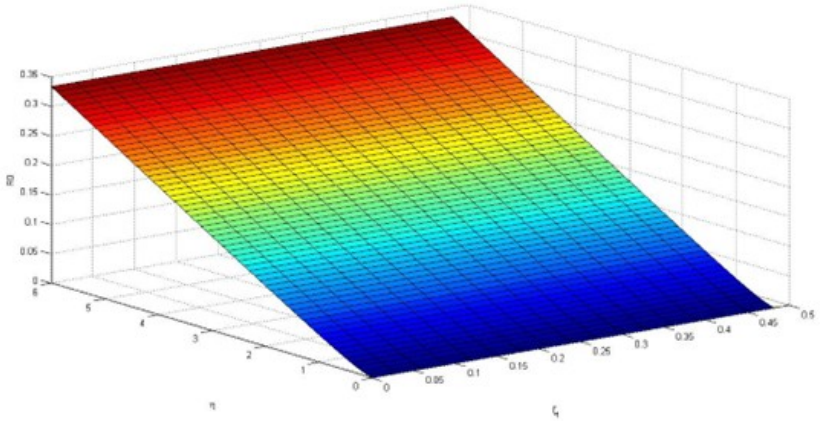

Figure 7. Global convergence trajectories tracing asymptotic leveling within the Fully Recovered (R_2) compartment.

5. Discussion

The model fitting was carried out using a function optimizer in MATLAB, which provided the initial parameter estimates required for the "fmincon" function in MATLAB's Optimization Toolbox. The Gillespie Algorithm, implemented in R, was applied to fitting the stochastic model and to analyze the continuous dynamic behavior of the individual compartments.

The model fitting was conducted for the epidemic period starting from September 2017, when the index case in Nigeria was reported, through August 25, 2024. Based on the available data for the daily cumulative confirmed cases, we estimate the values of the parameters τ, α, π_1, π_2, ζ_1, θ, and the initial conditions $E(0)$, $P_v(0)$, $F_v(0)$. It is important to note that both π_2 and τ were set at zero because, during the study period, neither the rate at which the infectious class was fully vaccinated nor the rate at which the susceptible class was directly fully vaccinated were actively implemented in public health policy fields. The remaining model parameters used for all operational runs are provided in Table 2. Figure 5 demonstrates that the tracking model aligns well with real Nigerian data sets for the monthly cumulative confirmed MPOX cases.

Figures 2 and 3 illustrate the explicit trends observed in the main population compartments. For the susceptible population (S), there is an initial rapid decline, indicating the rapid spread of the disease transmission, followed by eventual stabilization as the community paths settle. In the exposed class (E), the number of individuals increases until it reaches a peak around the 10th month, followed by a gradual decline, indicating that the disease progress is coming under control. In the infectious class (I), the count initially grows rapidly, reaching its peak near the 15th month before experiencing a steady decrease.

The partially vaccinated population (P_v) shown in Figure 4 exhibits a flat general trend, indicating that partial immunity individuals lose protection over time and become susceptible again due to the short-term single-dose efficacy of the vaccine. In contrast, the fully vaccinated population (F_v) within Figure 5 shows a gradual initial increase, reflecting higher rates of adherence to the vaccine, with a subsequent decrease showing that the complete vaccination campaign successfully minimizes the active host pool. The tracking paths across recovered classes (R_1 and R_2) detailed in Figures 6 and 7 verify that the disease parameters support overall epidemic control over an extended period of time.

The basic reproduction number (R_0) plays a crucial role in understanding disease expansion or elimina-

tion thresholds. To explore the effect of various transmission parameters on R_0, a series of multi-dimensional threshold surface plots were generated. When examining how R_0 changes with variations in the transmission rate (α) and the rate at which exposed individuals become fully vaccinated (ε), increases in both ε and α drop R_0 values significantly. This implies that higher proactive tracking from exposed individuals, coupled with a faster full vaccination rate, restricts the spread of the disease and drives R_0 below the crucial unity threshold.

Further parametric evaluations demonstrate the relationship between the proportion of fully recovered individuals ζ_2, the natural death rate (η), and the threshold variable R_0. As ζ_2 increases along the operational axis, R_0 decreases significantly, indicating that higher complete recovery rates reduce the number of individuals capable of spreading the disease. Additionally, shifts in the baseline mortality rates further impact active transmission potential, establishing clear conditions under which targeted pharmaceutical intervention profiles effectively suppress long-term virus circulation.

5.1. Parameter Limitations and Generalizability Concerns

During the primary calibration of the model, the structural parameters τ (the rate of therapeutic or clinical failure leading to diagnostic regression) and π_2 (the breakthrough infection rate of fully vaccinated individuals exhibiting immediate clinical symptoms) were fixed to zero ($\tau = 0, \pi_2 = 0$). This constraint was mathematically necessary to prevent over-parameterization and numerical instability during optimization against the available regional surveillance data, which reported negligible breakthrough rates within the localized observation window.

However, fixing these boundaries carries clear implications for the model's generalizability. Assuming $\tau = 0$ implies perfect recovery retention post-treatment, whereas assuming $\pi_2 = 0$ implies absolute temporary shielding against immediate symptomatic onset post-booster. In broader geographic contexts—particularly where highly divergent viral clades (e.g., Clade I vs. Clade II) co-circulate or where high sub-populations of immunocompromised individuals exist—these parameters will deviate from zero. Consequently, while the zero-value allocation preserves local predictive power, model deployment to broader international frameworks must relax these boundaries to accommodate potential vaccine escape mutations and therapeutic failures.

6. Conclusion

A non-linear compartmental model has been developed to provide insights into the transmission dynamics of MPOX disease. This model includes seven compartments, introducing partial vaccination (P_v), full vaccination (F_v), recovery with partial immunity (R_1), and recovery with full immunity (R_2), which extend beyond classical epidemiology setups. The basic reproduction number (R_0) was calculated using the next-generation matrix method. We derived the disease-free equilibrium, endemic equilibrium, and determined the stability conditions.

Through numerical simulations, we demonstrated how various parameters impact the basic reproduction number, R_0. The results indicate that partial vaccination alone is insufficient for long-term disease control, while full vaccination proves highly effective in managing the spread. The simulations highlight the critical role full vaccination regimens play in successfully controlling the MPOX virus.

Conflict of Interest

The authors declare that they do not have any conflict of interest.

Author Credit Statement

C.U.C. (Chinelo U. Chikwelu): Conceptualization; Methodology; Formal analysis; Investigation; Writing – Original Draft.
S.U.E. (Samuel U. Enogwe): Methodology; Software; Validation; Formal analysis.
C.G.O. (Chinwe G. Okoye): Methodology; Data Curation; Writing – Review & Editing.
O.J.O. (Okechukwu J. Obulezi): Conceptualization; Methodology; Software; Supervision; Project administration; Writing – Review & Editing.

Data Availability Statement

The data used in this study are simulated and are within the manuscript.

References

1.Alakunle, E., Moens, U., Nchinda, G., and Okeke, M. I. (2020). Monkeypox virus in nigeria: infection biology, epidemiology, and evolution. *Viruses*, 12(11):1257.

2.Bankuru, S. V., Kossol, S., Hou, W., Mahmoudi, P., Rychtář, J., and Taylor, D. (2020). A game-theoretic model of monkeypox to assess vaccination strategies. *PeerJ*, 8:e9272.

3.Bhunu, C., Garira, W., and Magombedze, G. (2009). Mathematical analysis of a two strain hiv/aids model with antiretroviral treatment. *Acta biotheoretica*, 57(3):361–381.

4.Durski, K. N., McCollum, A. M., Nakazawa, Y., Petersen, B. W., Reynolds, M. G., Briand, S., Djingarey, M. H., Olson, V., Damon, I. K., and Khalakdina, A. (2018). Emergence of monkeypox—west and central africa, 1970–2017. *MMWR. Morbidity and mortality weekly report*, 67.

5.Elsonbaty, A., Adel, W., Aldurayhim, A., and El-Mesady, A. (2024). Mathematical modeling and analysis of a novel monkeypox virus spread integrating imperfect vaccination and nonlinear incidence rates. *Ain Shams Engineering Journal*, 15(3):102451.

6.Gessain, A., Nakoune, E., and Yazdanpanah, Y. (2022). Monkeypox. *New England Journal of Medicine*, 387(19):1783–1793.

7.Grant, R., Nguyen, L.-B. L., and Breban, R. (2020). Modelling human-to-human transmission of monkeypox. *Bulletin of the World Health Organization*, 98(9):638.

8.Hutson, C. L., Gallardo-Romero, N., Carroll, D. S., Clemmons, C., Salzer, J. S., Nagy, T., Hughes, C. M., Olson, V. A., Karem, K. L., and Damon, I. K. (2013). Transmissibility of the monkeypox virus clades via respiratory transmission: investigation using the prairie dog-monkeypox virus challenge system. *PLoS One*, 8(2):e55488.

9.Jezek, Z., Szczeniowski, M., Paluku, K., Mutombo, M., and Grab, B. (1988). Human monkeypox: confusion with chickenpox. *Acta tropica*, 45(4):297–307.

10.Kantele, A., Chickering, K., Vapalahti, O., and Rimoin, A. (2016). Emerging diseases—the monkeypox epidemic in the democratic republic of the congo. *Clinical Microbiology and Infection*, 22(8):658–659.

11.Kraemer, M. U., Tegally, H., Pigott, D. M., Dasgupta, A., Sheldon, J., Wilkinson, E., Schultheiss, M., Han, A., Oglia, M., Marks, S., et al. (2022). Tracking the 2022 monkeypox outbreak with epidemiological data in real-time. *The Lancet Infectious Diseases*, 22(7):941–942.

12.Lahariya, C., Thakur, A., and Dudeja, N. (2022). Monkeypox disease outbreak (2022): epidemiology, challenges, and the way forward. *Indian pediatrics*, 59(8):636–642.

13.Mahase, E. (2022). Monkeypox: What do we know about the outbreaks in europe and north america?

14.Molla, J., Sekkak, I., Ortiz, A. M., Moyles, I., and Nasri, B. (2023). Mathematical modeling of mpox: A scoping review. *One Health*, 16:100540.

15.Mushayabasa, S. (2011). Modelling the transmission dynamics of pox-like infections. *IAENG International Journal of Applied Mathematics*, 41(2).

16.Nguyen, P.-Y., Ajisegiri, W. S., Costantino, V., Chughtai, A. A., and MacIntyre, C. R. (2021). Reemergence of human monkeypox and declining population immunity in the context of urbanization, nigeria, 2017–2020. *Emerging Infectious Diseases*, 27(4):1007.

17.Odom, M. R., Hendrickson, R. C., and Lefkowitz, E. J. (2009). Poxvirus protein evolution: family wide assessment of possible horizontal gene transfer events. *Virus research*, 144(1-2):233–249.

18.Peter, O. J., Kumar, S., Kumari, N., Oguntolu, F. A., Oshinubi, K., and Musa, R. (2022). Transmission dynamics of monkeypox virus: a mathematical modelling approach. *Modeling Earth Systems and Environment*, 8(3):3423–3434.

19.Peter, O. J., Viriyapong, R., Oguntolu, F. A., Yosyingyong, P., Edogbanya, H. O., and Ajisope, M. O. (2020). Stability and optimal control analysis of an scir epidemic model. *J. Math. Comput. Sci.*, 10(6):2722–2753.

20.Reynolds, M. G., Carroll, D. S., and Karem, K. L. (2012). Factors affecting the likelihood of monkeypox's emergence and spread in the post-smallpox era. *Current Opinion in Virology*, 2(3):335–343.

21.Somma, S. A., Akinwande, N. I., and Chado, U. D. (2019). A mathematical model of monkey pox virus transmission dynamics. *Ife Journal of Science*, 21(1).

22.TeWinkel, R. E. (2019). *Stability analysis for the equilibria of a monkeypox model*. PhD thesis, The University of Wisconsin-Milwaukee.

23.USMAN, S. H. (2017). Modeling the transmission dynamics of the monkeypox virus infection with treatment and vaccination interventions. *Journal of Applied Mathematics and Physics*, 5:2335–2353.